frontiers | Frontiers in Earth Science

TYPE Original Research
PUBLISHED 10 January 2024
DOI 10.3389/feart.2023.1353050

OPEN ACCESS

EDITED BY
Chang Zhang,
Chinese Academy of Sciences (CAS), China

REVIEWED BY
Ya Sun,
Central South University, China
Tuo Zheng,
Nanjing Tech University, China

*CORRESPONDENCE
Yuan Gao,
qzgyseis@163.com

RECEIVED 09 December 2023
ACCEPTED 27 December 2023
PUBLISHED 10 January 2024

CITATION
Wang A-J and Gao Y (2024), Possible layered lithospheric anisotropy around Longmenshan Faults by teleseismic S wave splitting and receiver functions.
Front. Earth Sci. 11:1353050.
doi: 10.3389/feart.2023.1353050

Possible layered lithospheric anisotropy around Longmenshan Faults by teleseismic S wave splitting and receiver functions

An-Jian Wang and Yuan Gao*

Key Laboratory of Earthquake Prediction, Institute of Earthquake Forecasting, China Earthquake Administration, Beijing, China

This study conducts an in-depth analysis of seismic anisotropy around the Longmenshan Faults. Utilizing a dataset of about 7710 earthquake catalogs from July 2007 to March 2023, we applied S wave splitting and receiver function methods to examine Pms and XKS waveforms collected from 12 fixed broadband stations across Gansu and Sichuan provinces. Our analysis revealed significant variations in seismic anisotropy between the crust and lithosphere, marked by distinct fast wave directions and delay times. These characteristics point to the possibility for layered anisotropy within the region. A two-layer anisotropy inversion analysis at key stations further delineated the differential anisotropic behaviors between the crust and the upper mantle, underscoring the impact of local geological structures and mantle dynamics. Crucially, our study posits the existence of layered anisotropy around the Longmenshan Fault Zone, a finding that significantly advances our comprehension of the region's seismic anisotropy and adds a vital dimension to our understanding of its subsurface structural intricacies and tectonic evolution.

KEYWORDS

anisotropy, teleseismic S wave splitting, lithospheric deformation, receiver fuctions, longmenshan faults

Introduction

The study of the Tibetan Plateau, a region characterized by intense seismic activity and tectonic dynamics within mainland China, is pivotal for comprehending internal continental deformation, deep material migration, and tectonic evolution. The interaction between the Indian and Eurasian Plates has resulted in significant uplift and thickening of the plateau. This process is accompanied by the eastward migration of deep crustal and mantle materials, impeded markedly upon encountering the Sichuan Basin. Such geological phenomena have been the focus of considerable interest in the geoscience community. Research into the deep material movement within the plateau predominantly revolves around three hypotheses: the rigid extrusion model (Tapponnier et al., 2001), the medium continuous deformation model (England and Houseman, 1986), and the lower crustal flow model (Royden et al., 1997; 2008). Each of these hypotheses highlights distinct aspects, such as fault activity, coherent crust-mantle deformation, and material flow within the lower crust, thereby underscoring the complexity beneath the plateau's surface.

Situated at the interface of the eastern Tibetan Plateau's Songpan-Ganzi orogenic belt and the Sichuan Basin, the Longmenshan Fault Zone represents a transitional region

between the active Tibetan Plateau block and the stable Yangtze Craton , as illustrated in Figure 1. This zone exhibits profound differences in topography, geological structure, and deeper stratigraphy on either side (Burchfiel et al., 1995). The eastward movement of the plateau is significantly hindered by the Sichuan Basin's rigid lithosphere, leading to a marked deceleration of crustal movement within the fault zone, subsequent uplift of the crustal base, and an increase in crustal thickness. Characterized by northeast-trending, west-dipping reverse faults such as the Back Mountain, Central, and Front Mountain faults, the Longmenshan Fault Zone exhibits a combination of thrusting and right-lateral strike-slip movements, with clear zonation and segmentation along its dip and strike (Yang et al., 2021). GPS data reveal drastic lateral variations in crustal velocity structure, indicative of deep heterogeneity. These tectonic complexities and deep dynamical processes have been the driving forces behind significant seismic events, including the 2008 Wenchuan Ms8.0 and 2013 Lushan Ms7.0 earthquakes. Various models have been proposed to explain the fault zone's deformation patterns, including the upper crustal brittle shortening model by Tapponnier et al. (2001) and the combined brittle upper crust and ductile middle-lower crust with a mid-lower crustal ductile channel flow (Burchfiel et al., 2008; Royden et al., 2008; Robert et al., 2010). Although southeastward lower crustal flow at the plateau's southeastern edge has been substantiated through seismological evidence (Sun et al., 2012; Bao et al., 2015), direct evidence of crustal flow in the Longmenshan Fault Zone remains elusive, warranting further in-depth exploration of crust-mantle velocity structures and anisotropy characteristics.

Seismic anisotropy serves as a crucial tool for investigating the Earth's internal deformation characteristics. When shear waves travel through an anisotropic medium, they split into fast and slow components with distinct velocities and nearly orthogonal polarization directions, a phenomenon well-documented by Crampin (1978, 1981). This directional dependency of wave velocity is a hallmark of seismic anisotropy, which can be categorized into Shape Preferred Orientation (SPO) and Lattice Preferred Orientation (LPO) anisotropy. The former arises from variations in elastic parameters across layered media, while the latter is due to differential orientations of mineral crystals. The upper crust's anisotropy is primarily sourced from EDA (Extensive-Dilatancy Anisotropy) microcrack structures (Crampin, 1984). These fluid-inclusive EDA microcracks, widely present in the crust, align under compressive stress, correlating the fast wave polarization with the regional principal stress field (Crampin, 1981). Besides EDA microcracks, the middle and lower crust's anisotropy may also originate from the preferential alignment of minerals and melts within rocks (Barruol and Mainprice, 1993). In the upper mantle, anisotropy is mainly due to lattice preferred orientations of minerals like olivine (Christensen and Yuen, 1984; Silver and Chan, 1991), contributing to our understanding of crust-mantle deformation characteristics and mantle flow mechanisms.

The splitting of the P-to-S converted phase (Pms phase), confined to the crust, eliminates the influence of deep mantle anisotropy, thus reflecting the deformation and anisotropy across the entire crustal thickness. In contrast, teleseismic phases SKS, PKS,

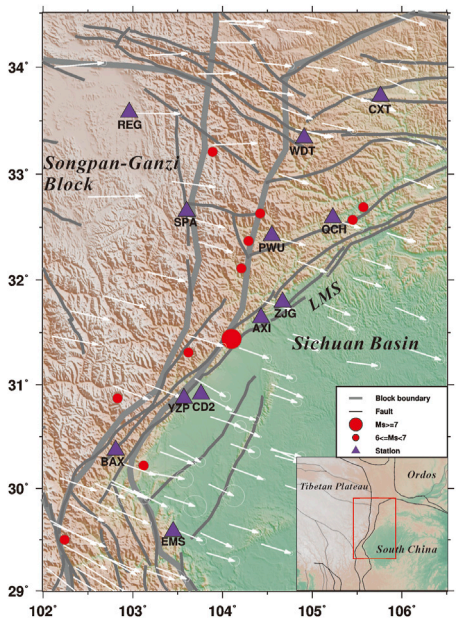

FIGURE 1
Distribution of major faults, seismic stations in the study area. LMS:Longmenshan Fault. White arrows indicate regional GPS velocity vectors (from Wang and Shen, 2020; The reference system is the Eurasian plate).

and SKKS (shortly XKS) splitting traditionally interpreted as representing lithosphere and asthenosphere top anisotropy (Silver, 1996), also integrates information on both crustal and upper mantle anisotropy in regions with thick, anisotropic crusts. By comparing Pms and XKS wave splitting parameters at the same location, we can explore the presence of coupling or layered anisotropy between the crust and mantle and discern the relative contributions of the crust and upper mantle in lithospheric deformation. This analytical method offers novel insights into regional geological structures and dynamics, particularly in terms of crust-mantle layering characteristics. Integrating these waveform data enables a more comprehensive revelation of Earth's internal structure and dynamical processes, thereby enriching our understanding of the intricate interplays within the Earth's interior.

Numerous researchers have previously investigated the crustal and mantle anisotropy in the Longmenshan area, contributing to a growing body of knowledge in this field (Gao et al., 2014; Gao et al., 2018). Research in the Longmenshan Fault Zone has yielded various results for the splitting parameters of both Pms and XKS waves, including the fast wave polarization directions (short for FPDs) and delay time, as illustrated in Figure 2. Sun et al. (2011) identified the FPDs in the Longmenshan Fault Zone area as predominantly NNE-oriented. Chen et al. (2013) observed that the FPD of crustal anisotropy in the region exhibit a notable clockwise rotation around the eastern Himalayan syntaxis, diverging from the patterns indicated by GPS motions. Zheng et al. (2018) reported that in the northern and southern parts of the Longmenshan Fault Zone, the FPDs are primarily NW-oriented, perpendicular to the fault strike, while in the central part, they are NE-oriented, parallel to the fault strike. In terms of XKS waves, the consensus is that the

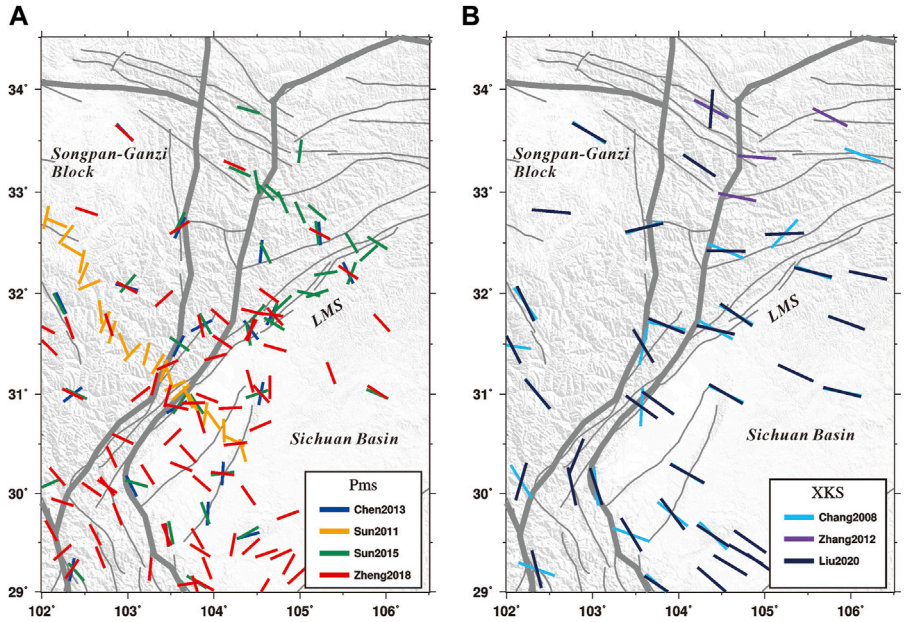

FIGURE 2
Results of Pms **(A)** and XKS **(B)** wave anisotropy in the Longmenshan Faults area by various researchers (Chen et al., 2013; Sun et al., 2011; Zheng et al., 2018; Sun et al., 2015; Chang et al., 2008; Zhang et al., 2012a; Liu et al., 2020).

predominant FPD aligns with the NW-SE orientation, consistent with the crustal motion velocity field measured by GPS. Additionally, complex anisotropy has been observed at certain stations, indicating a more intricate subsurface structure.

Data and method

In this study, we analyzed a comprehensive dataset comprising approximately 7,710 earthquake catalogs with magnitudes $M \geq 5.5$, spanning from July 2007 to March 2023, covering nearly 15 years. The event waveforms were extracted from the continuous waveform data, cut from 30 s before to 2,100 s after the theoretical P-wave arrival time. These waveforms were sourced from 12 broadband permanent stations belonging to CEA regional seismic networks in Gansu and Sichuan Province. For the analysis of Pms waves, data with epicentral distances ranging from 30 to 90° were selected, while for XKS waves, the range was widened to 30–180°. The original sampling rate of all data was 100 Hz. The filtering of the seismograms varied between the datasets: a 0.05–1.0 Hz bandpass filter was applied to the Pms data, whereas the XKS data underwent filtering within the 0.04–0.5 Hz range.

The receiver functions in this study were obtained by the time-domain iterative deconvolution technique (Ligorría and Ammon, 1999) with a Gaussian parameter of 5.0. Quality selection of RFs was based on two SNR criteria:To eliminate receiver functions with significant pre-arrival noise, we rejected any receiver function where $S_1 < 1.5$. Here, $S_1 = \frac{max|A_S|}{max|A_n|}$, with $max|A_S|$ and $max|A_n|$ defined as the maximum absolute values in the receiver function in the 1-s window around the P wave arrival and in the 1–10 s pre-arrival window, respectively. Subsequently, to filter out receiver functions with abnormal arrivals in the P wave coda, we excluded any receiver function where $S_2 < 1.2$. S_2 is calculated similarly to S_1, but $max|A_n|$ is the maximum absolute value from 7 s after the direct P wave to the end of the receiver function, avoiding the P-to-S converted phase from the Moho. To further ensure the reliability and robustness of our analysis, a meticulous visual inspection, as elaborated in Shi et al. (2023), was conducted on the receiver functions.

About 2,127 earthquake event records were used in the calculation of the receiver function. Figure 3 shows examples of Pms wave splitting calculation at CXT and ZJG station.

Meanwhile, for XKS wave splitting, we employed a method (Gao and Liu, 2014; Kong et al., 2018) focused on minimizing tangential energy, which involved a grid search analysis to determine the apparent FPD and delay time for each seismic record. The goal was to optimize parameters to reduce the tangential component energy post-correction to the lowest possible level, ideally zero, which aligns with the theory that anisotropy correction should result in a near-linear particle motion trajectory. Figure 4 demonstrates examples of single-layer anisotropy XKS wave splitting calculation at CXT and ZJG station using seismic records. In this study, 271 teleseismic events picked up clear phases XKS and were used to obtain anisotropic parameters.

Results

Employing the analysis methods described previously, we obtained the splitting parameters of Pms and XKS waves from

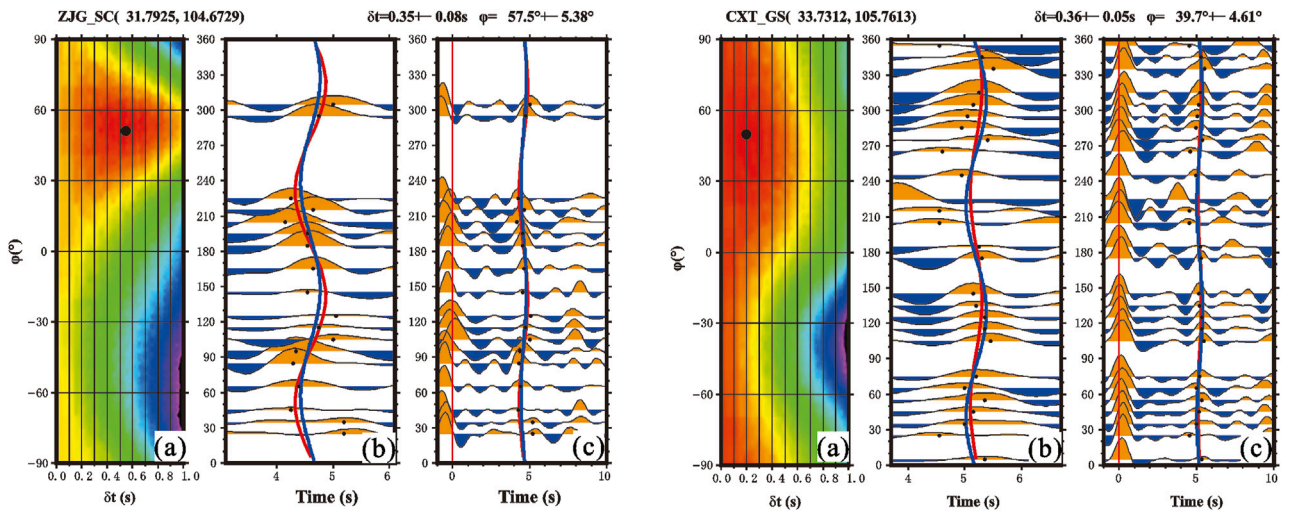

FIGURE 3
Pms wave splitting calculation at CXT and ZJG station.

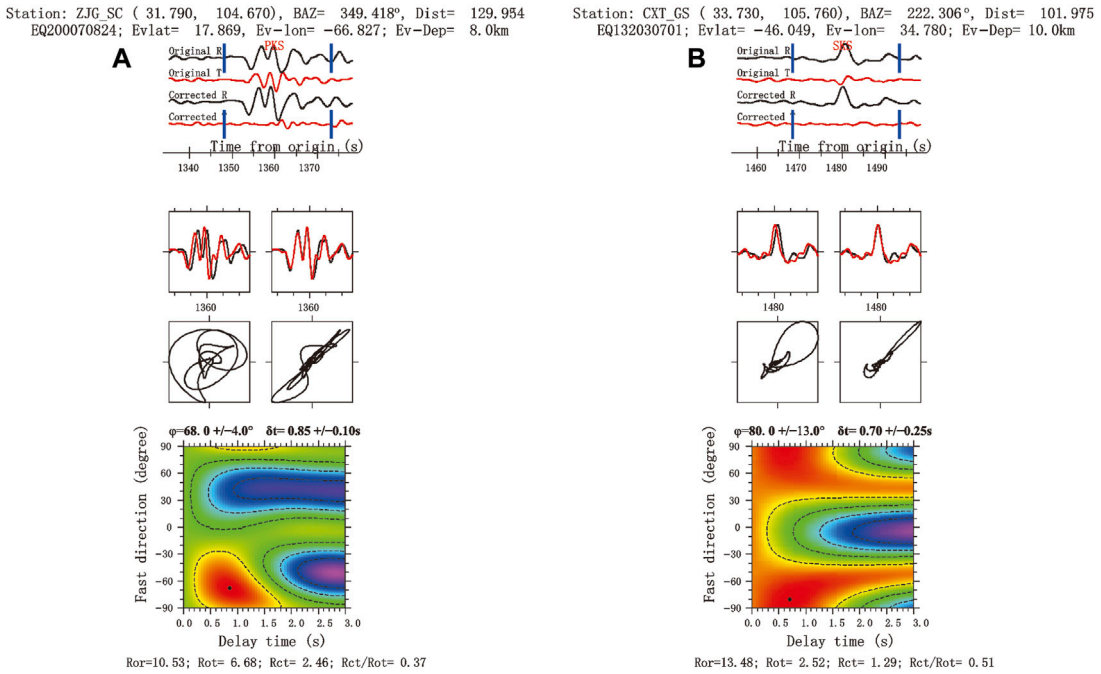

FIGURE 4
XKS wave splitting calculation at ZJG **(A)** and CXT **(B)** station.

12 fixed stations around the Longmenshan Fault Zone (as shown in Figure 5; Table 1).

The splitting times for Pms waves range from 0.08 to 1.13 s, with an average of 0.54 s. This significant variation in Fast Polarization Direction (FPD) and delay time across the region underscores the high degree of structural complexity. Within the Songpan-Ganzi block, the FPDs at some stations (REG, WDT, SPA) are predominantly NW-oriented, while at others (PWU, QCH, CXT), they are NE-oriented. Near the Longmenshan Fault Zone, at the junction between the Songpan-Ganzi block and the Sichuan Basin, most stations exhibit NE-oriented FPDs, parallel to the fault zone, with some (like BAX) showing NW orientations, perpendicular to the fault. Apart from a few stations like QCH with shorter delay times (0.08s), the majority exhibit longer delay times.

The splitting times for XKS waves range from 0.83 to 1.47 s, averaging 1.10 s. Notably, there are distinct differences in FPDs between the Tibetan Plateau and the Sichuan Basin, highlighting distinct anisotropic characteristics in these areas. In the eastern edge of the Tibetan Plateau, within the Songpan-Ganzi block, FPDs are generally NE or EW-oriented, whereas near the Longmenshan Fault

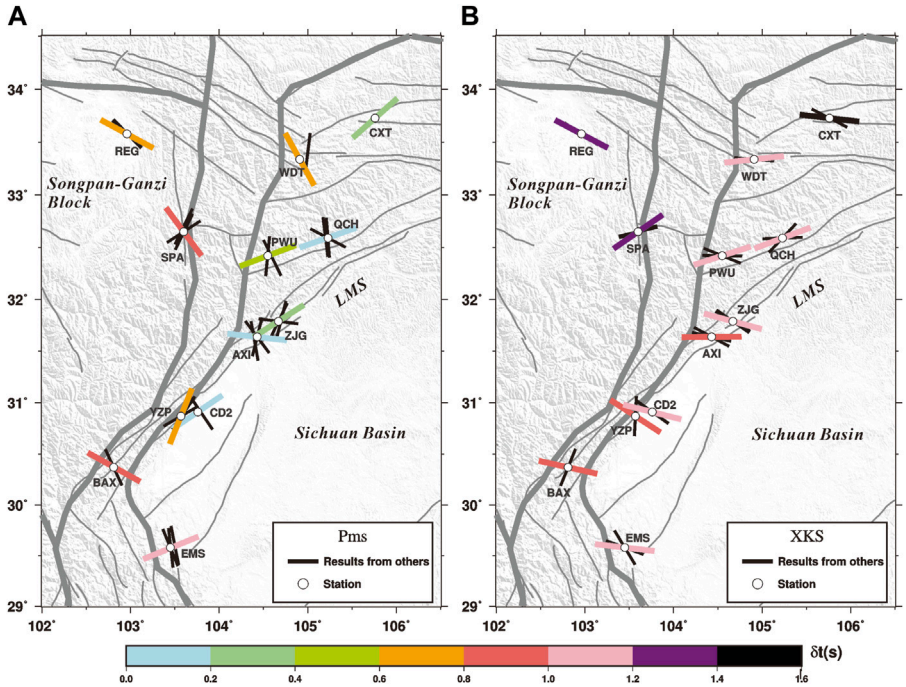

FIGURE 5
Results of Pms **(A)** and XKS **(B)** wave anisotropy in the Longmenshan Faults area obtained in this study.

TABLE 1 Pms and XKS wave anisotropy of each stations.

Station	φ (Pms)	δt (Pms)	φ (XKS)	δt (XKS)	Items (Pms)	Items (XKS)
AXI	−83.66	0.15	89.56	0.87	160	18
BAX	−59.91	0.56	53.44	0.96	125	9
CD2	30.96	0.30	104.36	1.14	93	14
CXT	48.2	0.30	96.62	1.47	194	13
EMS	67.54	1.13	96.69	1.02	114	13
PWU	69.3	0.56	72.02	1.02	206	43
QCH	70.52	0.08	69.35	1.04	297	34
REG	118.5	0.69	118.00	1.38	383	32
SPA	143.7	0.90	55.19	1.35	85	31
WDT	151.10	0.68	83.69	1.07	174	36
YZP	21.68	0.69	123.25	0.83	165	12
ZJG	57.24	0.40	105.12	1.14	131	16

Zone and at the block boundary, FPDs are predominantly NWW-oriented. The delay times in these regions are relatively consistent with minimal fluctuations.

Figure 6A presents the distribution of stations along the Longmenshan Fault Zone and in the adjacent Songpan-Ganzi block, illustrating significant disparities in crustal and lithospheric anisotropy. This pattern of variation is particularly evident near the Longmenshan Fault Zone, providing a fundamental basis for discussing the layered characteristics of the region's structure. The observed variations in anisotropic parameters, especially the distinct differences in FPDs and delay times between the crustal and lithospheric levels, suggest a complex interplay of tectonic forces and material compositions in these areas.

Discussions

Stations within the Songpan-Ganzi block, particularly the REG station, exhibit NW-oriented FPDs for both crustal and lithospheric anisotropy, aligning with the principal stress direction within the

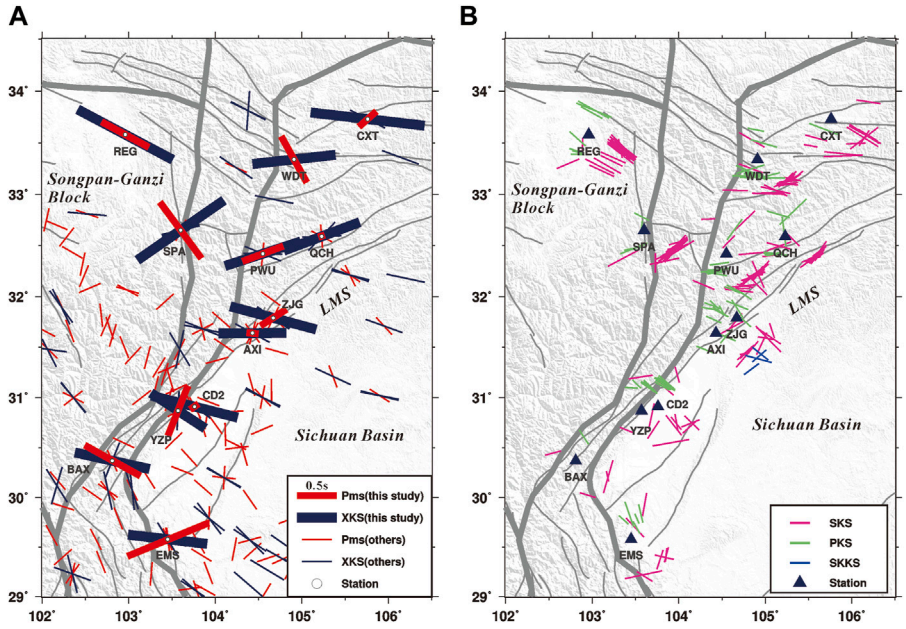

FIGURE 6
(A) Comparison of Pms and XKS results obtained in this study, and with the findings of other researchers. **(B)** Anisotropy parameters of XKS at 200 km piercing points projected to the surface.

block. The PWU and QCH stations, located on the Pingwu-Qingchuan Fault, show consistency in NE-oriented FPDs for both crust and lithosphere, parallel to the fault strike. This suggests potential vertical coherence in deformation across the crust and upper mantle at these stations. Interestingly, the Pms results we obtained for the PWU and QCH stations show variations when compared to the findings of Chen et al. (2013), Sun et al. (2015) and Zheng et al. (2018). Specificly, our results are broadly similar to those of other researchers in terms of delay time, but show significant differences in the FPDs. This discrepancy could be attributed to the more extensive dataset utilized in our study, encompassing 15 years and 2,127 effective recordings, which likely enhances the reliability of our results.

Stations AXI and ZJG, near the Guanxian-Jiangyou Fault, show variations in stress directions, as per *in-situ* stress results (Meng et al., 2013). The stress direction shifts from NE near ZJG to NWW-SEE towards AXI. The crustal FPDs at these stations align with these stress directions. At the AXI station, the FPDs for both Pms and XKS waves are essentially consistent, yet their splitting times are markedly different. This aspect might suggest that the mantle anisotropy predominantly characterizes the anisotropic properties beneath the station. The significant difference in crustal FPDs between AXI and ZJG, despite their close proximity (less than 40 km), indicates strong local deformation and heterogeneous anisotropic media distribution, possibly with layered characteristics. This is supported by crustal medium scattering intensity studies (Fan et al., 2016), which show distinct scattering wave field patterns between the two stations, implying significant underlying medium structural differences.

Stations YZP and CD2, south of the Longmenshan Fault, both exhibit NE-oriented crustal FPDs, suggesting strong influence from nearby faults. CD2 station shows lower crustal anisotropy intensity, with XKS wave fast directions primarily indicating upper mantle anisotropy. The close Pms and XKS wave splitting delay times at YZP indicate higher crustal anisotropy levels, but given the station's proximity to the Sichuan Basin edge, its complex waveforms (Zhang et al., 2008) could be influenced by the edge's sedimentary cover.

At BAX station, both crustal and lithospheric anisotropy FPDs are NW-oriented, consistent with the regional principal stress direction, reflecting the dynamic background of eastward compression from the Tibetan Plateau. The NE-oriented XKS results for BAX in Liu et al. (2020) differ from this study's findings. Indeed, when analyzing the BAX station, XKS waves from specific azimuthal coverages yielded directions similar to those reported by Liu. However, the results presented in this article represent a composite outcome derived from a well-covered azimuthal range. As illustrated in Figure 6B, the distribution of piercing points around our BAX station is relatively uniform. The presence of multiple dominant directions at this station, as suggested by these findings, may warrant further discussion and exploration.

Stations SPA (near the Longmenshan Fault in the Songpan-Ganzi block) and WDT (at the southeastern end of the West Qinling Fault Zone) show NW-oriented Pms wave FPDs, aligning with GPS motion fields and regional principal stress directions (Kan et al., 1977). The observed trend of XKS wave FPDs from NE to EW/NW from west to east (SPA, WDT, CXT) may reflect the asthenospheric flow pattern of the Tibetan Plateau material being squeezed by the Sichuan Basin along a channel beneath the Qinling. The NE-oriented Pms FPD at CXT, differing from structural stress directions, might be influenced by the nearby Lixian-Luojiaobao Fault.

Research on Moho depth (Jiang et al., 2012) indicates a westward sloping and gradual descent of the Moho beneath the western margin of the Yangtze Platform, with depths varying between 40–48 km and an average crustal wave speed ratio of

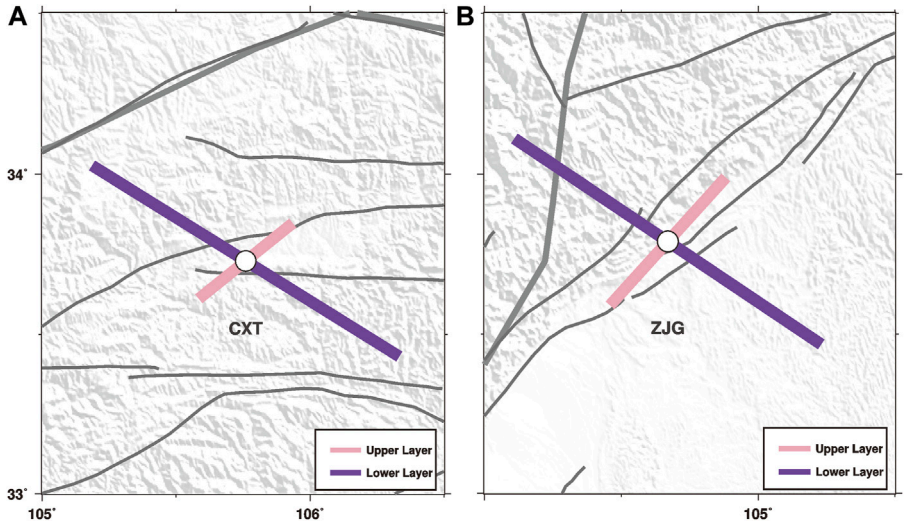

FIGURE 7
Two-layer anisotropy calculation of station CXT **(A)** and ZJG **(B)**.

TABLE 2 Two-layer anisotropy calculation of station CXT and ZJG.

Station	Pms	XKS	Upper layer	Lower layer
	φ(°)/δt(s)			
CXT	48.2/0.30	96.62/1.47	51.0/0.30	122.0/1.50
ZJG	57.24/0.30	105.12/1.14	42.0/0.70	124.0/1.50

1.8. In contrast, the Songpan-Ganzi block west of the Longmenshan Fault has an average crustal wave speed ratio of 1.76, with the Moho depth being approximately 10 km deeper in the south than in the north, showing a south-deep, north-shallow pattern. Evidence (Wang et al., 2016) suggests that inclined interfaces impact the calculation of anisotropy from receiver functions, potentially explaining unusual long Pms wave splitting delay times at some stations, like EMS.

Two-layer anisotropy

We employed the method proposed by Zuo and Niu (2019) for calculating two-layer anisotropy, focusing on stations in our study area where significant differences were observed between crustal and lithospheric anisotropy. This method contemplates the possibility of dual-layer anisotropy within the lithosphere, comprising both the crust and upper mantle. It uses an analogous two-layer theoretical model, treating the upper layer as the crust and the lower layer as the upper mantle. The method involves a grid search analysis of four splitting parameters: FPD and delay time for the upper (crustal) layer, and FPD and delay time for the lower (mantle) layer. The optimal two-layer anisotropy results correspond to the parameters where the objective function reaches its minimum value. This approach allows for a nuanced understanding of the distinct anisotropic behaviors between the crust and the upper mantle, providing a comprehensive view of the subsurface structural dynamics. The results are presented in Figure 7 and Table 2.

At station CXT, the crustal anisotropy FPD, as calculated from receiver functions, was oriented NE, while the lithospheric anisotropy direction calculated from XKS was NWW, showing a significant difference. This prompted a two-layer anisotropy inversion analysis. The inversion revealed an upper layer (crust) anisotropy at 51°/0.3s, closely aligning with the receiver function result of 48.2°/0.3s. The lower layer (lithospheric mantle) anisotropy was determined to be 122.0°/1.50s, approximating the XKS calculated result of 96.62°/1.47s. This suggests a realistic representation of the subsurface anisotropic characteristics.

In the middle to upper crust, anisotropy is primarily influenced by local structures such as faults and stress-induced medium deformations (e.g., oriented crack structures). The lower crust's anisotropy is more affected by factors like medium deformation, crystal alignment, and material flow. The upper layer anisotropy at station CXT may be associated with the nearby Lixian-Luojiaobao Fault, while the lower layer reflects the flow of upper mantle materials. Near-field S-wave inversion studies (Zhang et al., 2012b; Guo et al., 2015) have shown NW or NWW FPDs at CXT, which differ from our findings, possibly due to near-field S-wave splitting not reflecting mid-to-lower crustal anisotropy. This suggests the presence of anisotropic soft materials in the mid-to-lower crust at CXT, supporting the hypothesis of lower crustal flow in this region, where stress and strain from the crust and upper mantle may not be effectively transmitted.

At station ZJG, the crustal and lithospheric anisotropy directions were also markedly different, NE and NWW respectively. Two-layer anisotropy inversion at ZJG yielded an upper layer anisotropy of 42.0°/0.70s, closely matching the receiver function result of 57.24°/0.30s, and a lower layer anisotropy of 124.0°/1.50s, closely approximating the XKS result of 105.12°/1.14s. This again indicates a realistic representation of subsurface anisotropic features. As previously discussed, the ZJG region exhibits strong local deformation and uneven anisotropic media distribution, likely with layered characteristics. These results

validate this observation, further reinforcing the complexity and heterogeneity of subsurface structures in these areas.

Conclusion

This study presents a comprehensive analysis of seismic anisotropy in the region surrounding the Longmenshan Fault Zone, utilizing a dataset of approximately 7,710 earthquake catalogs spanning nearly 15 years. The analysis was conducted using both Pms and XKS waveforms from 12 broadband permanent stations in the study area, revealing significant variations in seismic anisotropy between the crust and lithosphere.

Our findings highlight the intricate tectonic dynamics of the region, with distinct FPDs and splitting times at various stations underscoring the complexity of the subsurface structures. Particularly, the two-layer anisotropy inversion analysis at stations CXT and ZJG indicates differences in anisotropic behaviors between the crust and the upper mantle, suggesting the influence of local structural features such as faults and the flow of upper mantle materials.

However, this study is not without its limitations. The inherent complexity of the regional structure and the limitations posed by station data coverage may affect the comprehensiveness of our findings. While our dataset is extensive, it cannot fully represent the entire region's seismic behavior, particularly in areas with sparse station coverage or complex geological features. Additionally, the assumptions and simplifications inherent in our modeling and inversion techniques may introduce uncertainties in our anisotropy estimations. So, it is necessary to conduct detailed research in the future with sufficient seismic waveform data.

Data availability statement

Publicly available datasets were analyzed in this study. This data can be found here: The teleseismic catalogs used in this study were obtained from USGS (https://www.usgs.gov/), and the waveform data were obtained from the International Earthquake Science Data Center (http://esdc.ac.cn/).

Author contributions

AW: Writing–original draft, Writing–review and editing. YG: Writing–review and editing.

Funding

The author(s) declare financial support was received for the research, authorship, and/or publication of this article. This study is supported by the National Natural Science Foundation of China (Project 42304073).

Acknowledgments

The teleseismic catalogs used in this study were obtained from USGS (https://www.usgs.gov/), and the waveform data were obtained from the International Earthquake Science Data Center (http://esdc.ac.cn/). The computational programs provided by Professors Stephan Gao, Kelly Liu, and Fansheng Kong for this study are gratefully acknowledged. Grateful to the guest editor Dr. Chang Zhang, two reviewers and the editorial office for their helpful and constructive comments.

Conflict of interest

The authors declare that the research was conducted in the absence of any commercial or financial relationships that could be construed as a potential conflict of interest.

Publisher's note

References

Bao, X., Sun, X., Xu, M., Eaton, D. W., Song, X., Wang, L., et al. (2015). Two crustal low-velocity channels beneath SE Tibet revealed by joint inversion of Rayleigh wave dispersion and receiver functions. *Earth Planet. Sci. Lett.* 415, 16–24. doi:10.1016/j.epsl.2015.01.020

Barruol, G., and Mainprice, D. (1993). A quantitative evaluation of the contribution of crustal rocks to the shear-wave splitting of teleseismic SKS waves. *Phys. Earth Planet. Interiors* 78 (3-4), 281–300. doi:10.1016/0031-9201(93)90161-2

Burchfiel, B. C., Royden, L. H., Van der Hilst, R. D., Hager, B. H., Chen, Z., King, R. W., et al. (2008). A geological and geophysical context for the Wenchuan earthquake of 12 May 2008, Sichuan, People's Republic of China. *GSA today* 18 (7), 4–11. doi:10.1130/gsatg18a.1

Burchfiel, B. C., Zhiliang, C., Yupinc, L., and Royden, L. H. (1995). Tectonics of the Longmen Shan and adjacent regions, central China. *Int. Geol. Rev.* 37 (8), 661–735. doi:10.1080/00206819509465424

Chang, L., Wang, C., and Ding, Z. (2008). Seismic anisotropy of upper mantle in Sichuan and adjacent regions. *Sci. China Ser. D Earth Sci.* 51 (12), 1683–1693. (in Chinese). doi:10.1007/s11430-008-0147-8

Chen, Y., Zhang, Z., Sun, C., and Badal, J. (2013). Crustal anisotropy from Moho converted Ps wave splitting analysis and geodynamic implications beneath the eastern margin of Tibet and surrounding regions. *Gondwana Res.* 24 (3-4), 946–957. doi:10.1016/j.gr.2012.04.003

Christensen, U. R., and Yuen, D. A. (1984). The interaction of a subducting lithospheric slab with a chemical or phase boundary. *J. Geophys. Res. Solid Earth* 89 (B6), 4389–4402. doi:10.1029/jb089ib06p04389

Crampin, S. (1978). Seismic-wave propagation through a cracked solid: polarization as a possible dilatancy diagnostic. *Geophys. J. Int.* 53 (3), 467–496. doi:10.1111/j.1365-246x.1978.tb03754.x

Crampin, S. (1981). A review of wave motion in anisotropic and cracked elastic-media. *Wave Motion* 3 (4), 343–391. doi:10.1016/0165-2125(81)90026-3

Crampin, S. (1984). Effective anisotropic elastic constants for wave propagation through cracked solids. *Geophys. J. Int.* 76 (1), 135–145. doi:10.1111/j.1365-246x.1984.tb05029.x

England, P., and Houseman, G. (1986). Finite strain calculations of continental deformation. l. Method and general results for convergent zones. 2.Comparison with the

India- Asia collision zone. *J. Geophys. Res. Solid Earth* 91 (B3), 3651–3676. doi:10.1029/JB091iB03p03664

Fan, X. P., Wang, J. F., Yang, C. J., Li, Q. H., He, Y. C., and Bi, X. M. (2016). Variations of the crust seismic scattering strength below the southeastern margin of the Tibetan plateau and adjacent regions. *Chin. J. Geophys.* 59 (7), 2486–2497. (in Chinese).

Gao, S. S., and Liu, K. H. (2014). Mantle transition zone discontinuities beneath the contiguous United States. *J. Geophys. Res. Solid Earth* 119 (8), 6452–6468. doi:10.1002/2014jb011253

Gao, Y., Shi, Y. T., and Chen, A. G. (2018). Crustal seismic anisotropy and compressive stress in the eastern margin of the Tibetan Plateau and the influence of the Ms 8.0 Wenchuan earthquake. *Chin. Sci. Bull.* 63 (19), 1934–1948. (in Chinese). doi:10.1360/n972018-00317

Gao, Y., Wang, Q., Zhao, B., and Shi, Y. (2014). A rupture blank zone in middle south part of Longmenshan Faults: effect after Lushan Ms 7.0 earthquake of 20 April 2013 in Sichuan, China. *Sci. China Earth Sci.* 57, 2036–2044. doi:10.1007/s11430-014-4827-2

Guo, G. H., Zhang, Z., Cheng, J. W., Dong, Z. P., Yan, J. P., and Ma, Y. W. (2015). Seismic anisotropy in the crust in northeast margin of Tibetan Plateau and tectonic implication. *Chin. J. Geophys.* 58 (11), 4092–4105. (in Chinese). doi:10.6038/cjg20151117

Jiang, X., Cheng, X. Q., Song, W. J., and Wang, C. (2012). Application of the H-Kappa method to invert the Moho depth and velocity ratio distribution in Longmenshan Fault Zone and its adjacent areas. *J. Inst. Disaster Prev.* 14 (3), 12–17. (in Chinese). doi:10.3969/j.issn.1673-8047.2012.03.003

Kan, R. J., Zhang, S. C., and Yan, F. T. (1977). A study on the characteristics of modern tectonic stress field and modern tectonic activity in Southwest China. *Acta Seismol. Sin.* 20 (2), 96–109. (in Chinese).

Kong, F., Wu, J., Liu, L., Liu, K. H., Song, J., Li, J., et al. (2018). Azimuthal anisotropy and mantle flow underneath the southeastern Tibetan Plateau and northern Indochina Peninsula revealed by shear wave splitting analyses. *Tectonophysics* 747, 68–78. doi:10.1016/j.tecto.2018.09.013

Ligorría, J. P., and Ammon, C. J. (1999). Iterative deconvolution and receiver-function estimation. *Bull. Seismol. Soc. Am.* 89 (5), 1395–1400. doi:10.1785/bssa0890051395

Liu, J., Wu, J., Wang, W., Fang, L., and Chang, K. (2020). Seismic anisotropy beneath the eastern margin of the Tibetan Plateau from SKS splitting observations. *Tectonophysics* 785, 228430. doi:10.1016/j.tecto.2020.228430

Meng, W., Chen, Q. C., Wu, M. L., Li, G. Q., Qin, X. H., and Feng, C. J. (2013). Research on segmentation and characteristic of tectonic stressfield of Longmenshan Fault Zone. *Prog. Geophys.* 28 (3), 1150–1160. (in Chinese). doi:10.6038/pg20130306

Robert, A., Zhu, J., Vergne, J., Cattin, R., Chan, L. S., Wittlinger, G., et al. (2010). Crustal structures in the area of the 2008 Sichuan earthquake from seismologic and gravimetric data. *Tectonophysics* 491 (1-4), 205–210. doi:10.1016/j.tecto.2009.11.010

Royden, L. H., Burchfiel, B. C., and Hilst, R. D. (2008). The geological evolution of the Tibetan Plateau. *Science* 321 (5892), 1054–1058. doi:10.1126/science.1155371

Royden, L. H., Burchfiel, B. C., King, R. W., Wang, E., Chen, Z. L., Shen, F., et al. (1997). Surface deformation and lower crustal flow in eastern Tibet. *Science* 276 (5313), 788–790. doi:10.1126/science.276.5313.788

Shi, Y., Gao, Y., Zhang, H., Zhang, Z., and Li, G. (2023). Crustal azimuthal anisotropy in the lateral collision zone of the SE margin of the Tibetan Plateau and its tectonic implications. *Geophys. J. Int.* 234 (1), 1–11. doi:10.1093/gji/ggad059

Silver, P. G. (1996). Seismic anisotropy beneath the continents: probing the depths of geology. *Annu. Rev. earth Planet. Sci.* 24 (1), 385–432. doi:10.1146/annurev.earth.24.1.385

Silver, P. G., and Chan, W. W. (1991). Shear wave splitting and subcontinental mantle deformation. *J. Geophys. Res. Solid Earth* 96 (B10), 16429–16454. doi:10.1029/91jb00899

Sun, C. Q., Chen, Y., and Gao, E. G. (2011). The crustal anisotropy and its geodynamical significance of the strong basin-range interaction zone beneath the east margin of Qinghai-Tibet plateau. *Chin. J. Geophys.* 54 (5), 1205–1214. (in Chinese). doi:10.3969/j.issn.0001-5733.2011.05.009

Sun, Y., Liu, J., Zhou, K., Chen, B., and Guo, R. (2015). Crustal structure and deformation under the Longmenshan and its surroundings revealed by receiver function data. *Phys. Earth Planet. Interiors* 244, 11–22. doi:10.1016/j.pepi.2015.04.005

Sun, Y., Niu, F., Liu, H., Chen, Y., and Liu, J. (2012). Crustal structure and deformation of the SE Tibetan plateau revealed by receiver function data. *Earth Planet. Sci. Lett.* 349, 186–197. doi:10.1016/j.epsl.2012.07.007

Tapponnier, P., Xu, Z., Roger, F., Meyer, B., Arnaud, N., Wittlinger, G., et al. (2001). Oblique stepwise rise and growth of the Tibet Plateau. *Science* 294, 1671–1677. doi:10.1126/science.105978

Wang, Q., Niu, F., Gao, Y., and Chen, Y. (2016). Crustal structure and deformation beneath the NE margin of the Tibetan plateau constrained by teleseismic receiver function data. *Geophys. J. Int.* 204 (1), 167–179. doi:10.1093/gji/ggv420

Xia, X. Y., and Gao, Y. (2024). Lithospheric deformation revealed by teleseismic phases SKS, PKS and SKKS splitting in the NE margin of the Tibetan Plateau. *Submitt. Front. Earth Sci.* 11. doi:10.3389/feart.2023.1342796

Yang, Y., Zhang, X., Hua, Q., Su, L., Feng, C., Qiu, Y., et al. (2021). Segmentation characteristics of the Longmenshan fault——constrained from dense focal mechanism data. *Chin. J. Geophys.* 64 (4), 1181–1205. (in Chinese). doi:10.6038/cjg2021O0286

Zhang, H., Gao, Y., Shi, Y. T., Liu, X. F., and Wang, Y. X. (2012a). Tectonic stress analysis based on the crustal seismic anisotropy in the northeastern margin of Tibetan plateau. *Chin. J. Geophys.* 55 (1), 95–104. (in Chinese). doi:10.6038/j.issn.0001-5733.2012.01.009

Zhang, H., Teng, J., Tian, X., Zhang, Z., Gao, R., and Liu, J. (2012b). Lithospheric thickness and upper-mantle deformation beneath the NE Tibetan Plateau inferred from S receiver functions and SKS splitting measurements. *Geophys. J. Int.* 191 (3), 1285–1294. doi:10.1111/j.1365-246x.2012.05667.x

Zhang, Y. J., Gao, Y., Shi, Y. T., and Cheng, W. Z. (2008). Shear-wave splitting of Sichuan regional seismic network. *Acta Seismol. Sin.* 21, 127–138. doi:10.1007/s11589-008-0004-z

Zheng, T., Ding, Z., Ning, J., Chang, L., Wang, X., Kong, F., et al. (2018). Crustal azimuthal anisotropy beneath the southeastern Tibetan Plateau and its geodynamic implications. *J. Geophys. Res. Solid Earth* 123 (11), 9733–9749. doi:10.1029/2018jb015995

Zuo, J., and Niu, F. (2019). Shear-wave splitting parameters of two-layer anisotropic media estimated from three different multilayer measurement methods. *Chin. J. Geophys.* 62 (8), 2885–2898. (in Chinese). doi:10.6038/cjg2019N0037